Safety Enforcement in Closed-Loop Anesthesia– A Comparison Study[☆,☆☆]

Mehdi Hosseinzadeh[a,*], Klaske van Heusden[b], Mahdi Yousefi[b], Guy A. Dumont[b], Emanuele Garone[c]

[a]*Department of Electrical and Systems Engineering, Washington University in St. Louis, St. Louis, Missouri, USA*
[b]*Department of Electrical and Computer Engineering, The University of British Columbia, Vancouver, Canada*
[c]*Service d'Automatique et d'Analyse des Systèmes, Université Libre de Bruxelles, Brussels, Belgium*

Abstract

This paper studies application of different constrained control concepts for the control of Depth of Hypnosis (DOH) in closed-loop anesthesia to guarantee patient safety, while ensuring acceptable tracking performance. The core idea is to formulate Overdosing (OD) prevention and Blood Pressure Decrease (BPD) prevention as operational constraints, and then use a constrained control scheme to enforce the constraints satisfaction at all times. In this paper, three methods are studied: 1) Explicit Reference Governor (ERG), 2) Safety Preserving Control (SPC), and 3) Model Predictive Control (MPC). The performance of the methods is assessed with respect to a simulated surgical procedure for 44 patients whose models have been identified using clinical data. In particular, three realistic clinical scenarios are studied in this paper: 1) normal mode, 2) stimulation, and 3) low clearance. The results demonstrate cons and pros of each method in closed-loop anesthesia according to clinically relevant assessments.

Keywords: Closed-loop anesthesia, Safety enforcement, Depth of hypnosis, Constrained control, Automated drug delivery.

1. Introduction

During surgical procedures, anesthesiologists continuously adjust the dosage of anesthetic drugs to reach an acceptable level of anesthesia. From a technical point of view, their actions can be interpreted as manual feedback control. Motivated by this observation, automated (closed-loop) administration of anesthetics has received increasing attention over the last two decades. Several articles have reported the technical and clinical aspects of this technology [1, 2, 3, 4, 5, 6, 7, 8].

To bring this technology to routine clinical practice, safety concerns associated with closed-loop anesthesia need to be addressed. One of the main safety concerns is drug overdosing which must be avoided during closed-loop anesthesia, despite inter-patient variability. Another concern is hypotension, as low blood pressure is common in the period following the induction of anesthesia [9, 10].

Several control schemes have been proposed to maintain patients' physiological variables within safe limits to avoid drug overdosing during closed-loop anesthesia [11, 12, 13, 14, 15, 16, 17, 18, 19, 20]. Constraints on blood pressure to avoid hypotension have also been considered [21, 22]. These schemes use varying control objectives, and are designed and evaluated using different models. The performance of the constrained control solutions is therefore confounded by design choices, variability in the models, and considered performance metrics. This work aims to provide a comprehensive comparison among three constrained control techniques, namely, Explicit Reference Governor (ERG), Model Predictive Control (MPC), and Safety-Preserving Control (SPC), which were previously proposed in the context of closed-loop anesthesia to avoid drug overdosing and hypotension [20, 22, 23]. To limit confounding factors, these methods are compared using the same model set, same safety constraints, and comparable unconstrained performance.

The above-mentioned techniques can employ the same constraints on physiological variables; however, their constrained-control objectives are different and they provide different levels of safety guarantees. For a given closed-loop system, ERG determines a dynamic auxiliary reference signal which gradually converges to the actual reference signal, while ensuring that the states remain within the safe region. MPC is a receding horizon control technique that solves a constrained optimization problem over a prediction horizon to find a feasible control input that satisfies the constraints, while optimizing control objectives. SPC, on the other hand, provides a formal proof of the existence of a control input (called safety-preserving) which maintains the states within the safe region. SPC calculates a subset of the constrained (safe) region or states, from which a safety-preserving controller exists.

We compare the performance and characteristics of the above-mentioned techniques in constrained closed-loop anesthesia, including constraints to avoid drug overdosing and hypotension. For this purpose, we employ a set of 44 patient models identified in [24] based on clinical data. Moreover, we com-

[☆]This research has been funded by the Fonds National de La Recherche Scientifique (FNRS)- Mandat d'Impulsion Scientifique (MIS): "Optimization-Free Control of Nonlinear Systems Subject to Constraints," Ref. F.4526.17.

[☆☆]The authors declare that there is no conflict of interest regarding the publication of this article.

[*]Corresponding author.

Email addresses: mehdi.hosseinzadeh@ieee.org (Mehdi Hosseinzadeh), klaskeh@ece.ubc.ca (Klaske van Heusden), mahdiyou@ece.ubc.ca (Mahdi Yousefi), guyd@ece.ubc.ca (Guy A. Dumont), egarone@ulb.ac.be (Emanuele Garone)

Nomenclature

AW	Anti Windup
BP	Blood Pressure
BPD	Blood Pressure Decrease
DOH	Depth of Hypnosis
DSM	Dynamic Safety Margin
ERG	Explicit Reference Governor
IT	Induction Time
LBM	Lean Body Mass
MPC	Model Predictive Control
NF	Navigation Field
OD	Overdosing
OS	Overshoot
PKPD	PharmacoKinetic-PharmacoDynamic
RT	Rise Time
SPC	Safety Preserving Control
ST	Settling Time
UDI	Used Drug for Induction

pare the closed-loop behaviour of these methods in three realistic clinical scenarios as proposed in [15]. We show that all three methods are capable of maintaining the system within the safety constraints during closed-loop anesthesia for all members of the 44-patient model set. However, there are significant differences in the transient responses. We conclude the paper by discussing the practical benefits and limitations of each method and the level of safety guarantee that each method provides. Contributions of this paper are: 1) to extend the ERG scheme proposed in [20] to prevent OD and BPD simultaneously, 2) to compare the performance of the three constrained control schemes in realistic clinical scenarios, and 3) to indicate how state-of-the-art constrained control methods need to be improved to meet performance requirements for clinical practice.

The rest of the paper is organized as follows. Section 2 describes the models used in the propofol delivery system. Section 3 describes the PID controller used as a precompensator. Design details of the ERG, SPC, and MPC are briefly discussed in Section 4, 5 and 6, respectively. In Section 7, simulations are carried out using the proposed schemes and comparison results are discussed. Finally, Section 8 provides concluding remarks.

2. Modeling of Pharmacological Effects of Propofol

The relationship between dose and pharmacological effects of administered anesthetic drug (propofol in this paper) can be described by the PharmacoKinetic-PharmacoDynamic (PKPD) model. The input to this process is the dose of administered drug, and the outputs are the clinical effect, in this paper the effect on DOH and BP in terms of the BPD.

The effect of propofol is commonly modeled using the following PKPD model, consisting of two parts: 1) the PK model, and 2) the PD model (see Figure 1). The PK model relates the drug plasma concentration with the administered dose. The PK model regarding the hypnotic effect can be expressed as

$$PK_H(s) = \frac{C_{p,H}(s)}{I(s)} = K_H \frac{(s+z_{1,H})(s+z_{2,H})}{(s+p_{1,H})(s+p_{2,H})(s+p_{3,H})}, \quad (1)$$

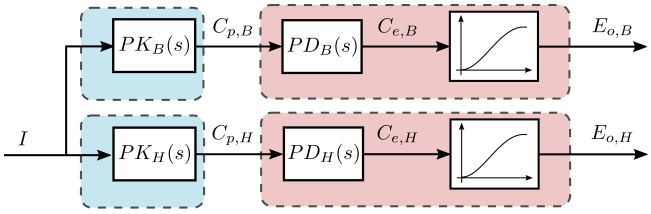

Figure 1: PKPD model block diagram.

where K_H, $z_{i,H}$, $i = 1,2$, and $p_{j,H}$, $j = 1,2,3$ are the gain, zeros, and poles of the model, respectively, and can be determined using, for example, the relations proposed by Schüttler and Ihmsen [25] or by Schnider *et al.* [26].

The PD model relates the plasma concentration with the pharmacological end-effect. In other words, the PD model describes the distribution of the propofol in the brain. For hypnotic effect, a first-order plus time-delay PD model is used as proposed by [24]:

$$PD_H(s) = \frac{C_{e,H}(s)}{C_{p,H}(s)} = e^{-T_d s} \frac{k_{d,H}}{s+k_{d,H}}, \quad (2)$$

where $C_{p,H}(t) = C_1(t)$, and T_d and $k_{d,H}$ are the transport delay and rate of propofol distribution between the plasma concentration and the brain, respectively. In addition, a nonlinear saturation function, called Hill function, is used to describe the relation between $C_{e,H}(t)$ and the clinical hypnotic effect $E_{o,H}(t)$, which is expressed as

$$E_{o,H}(t) = \frac{C_{e,H}(t)^{\gamma_H}}{EC_{50,H}^{\gamma_H} + C_{e,H}(t)^{\gamma_H}}, \quad (3)$$

where $EC_{50,H}$ is the steady-state plasma concentration to obtain 50% of the hypnotic effect, and γ_H is the cooperativity coefficient. Note that $E_{o,H}(t)$ is bounded between 0 and 1, where 0 means no hypnotic effect, and 1 is associated with the maximum effect of hypnosis that can be identified.

As discussed in [9], the PK model associated with BPD effect

can be expressed as

$$PK_B(s) = \frac{C_{p,B}(s)}{I(s)} = K_B \frac{(s+z_{1,B})(s+z_{2,B})}{(s+p_{1,B})(s+p_{2,B})(s+p_{3,B})}, \quad (4)$$

where K_B, $z_{i,B}$, $i = 1,2$, and $p_{j,B}$, $j = 1,2,3$ are the gain, zeros, and poles of the model, respectively. Also, the PD model describing the BPD effect can be expressed by the following first-order system

$$PD_B(s) = \frac{C_{p,B}(s)}{C_{e,B}(s)} = \frac{k_{d,B}}{s+k_{d,B}}, \quad (5)$$

preceding the following nonlinear saturation function

$$E_{o,B}(t) = \frac{C_{e,B}(t)^{\gamma_B}}{EC_{50,B}^{\gamma_B} + C_{e,B}(t)^{\gamma_B}}, \quad (6)$$

where $k_{d,B}$ is the rate of propofol distribution, $EC_{50,B}$ is the steady-state plasma concentration to obtain 50% of the effect on blodd pressure, and γ_B is the cooperativity coefficient. The percentage of the BPD can then be computed as $100 \cdot E_{o,B}(t)$.

Finally, the drug-pharmacological effect relationship of the propofol can be expressed by combining the PK models (1) and (4), and PD models (2)-(3) and (5)-(6) to come up with a PKPD model, as shown in Figure 1. It is assumed that the demographics are known and consequently the PK model (1) is known. For $PK_B(s)$, $PD_B(s)$ and the nonlinear function (6), we use the parameters provided in [9], which means that PD model (5)-(6) is assumed known. On the contrary, the PD model (2)-(3) is unknown and introduces significant inter-patient variability, since its parameters cannot be easily determined based on patient's characteristics. However, the parametric uncertainty is limited to an interval with known bounds.

3. Precompensating the System

Both ERG and SPC assume a precompensating (performance) controller is available, in this case for the control of DOH in closed-loop anesthesia. In this paper, we use the PID controller that has been clinically evaluated in over 100 cases [27]. The block diagram of the precompensating structure is shown in Figure 2. In the SPC and ERG solution, the system is compensated by this controller, and then augmenting it with an *add-on* unit to enforce constraints satisfaction.

This controller uses feedback from the NeuroSENSE monitor whose dynamics is usually modeled as a second-order low-pass filter [28]:

$$S(s) = \frac{Y_1(s)}{E_{o,H}(s)} = \frac{1}{(8s+1)^2}, \quad (7)$$

where $Y_1(s)$ is the Laplace transform of the WAV_{CNS} index, the cortical index that reflects the level of consciousness of the patient [29].

In the PID controller, the infusion rate $I(t)$ is calculated as

$$I(t) = k\left(v(t) - y_1(t)\right) + k_i \int \left(v(t) - y_1(t)\right) dt + k_d \left(0.8\frac{d}{dt}v(t) - \frac{d}{dt}y_1(t)\right), \quad (8)$$

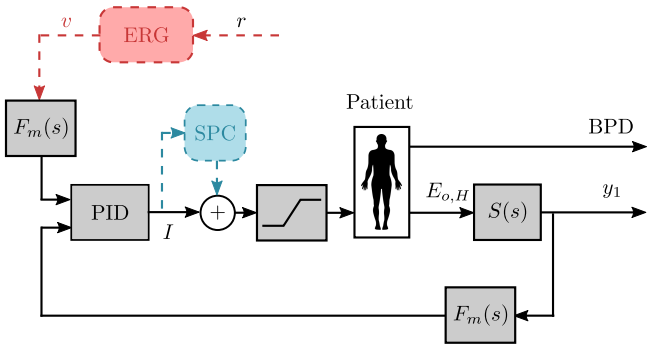

Figure 2: Block diagram of the precompensating control structure. Red lines and blocks are active only in ERG scheme, and blue lines and blocks are active only in SPC scheme.

where the parameters k, k_i, and k_d are calculated based on Lean Body Mass (LBM) which can be computed as [30]:

$$\begin{cases} \text{LBM} = 0.3281W + 0.33929H - 29.5336, & \text{if male} \\ \text{LBM} = 0.29569W + 0.41813H - 43.2933, & \text{if female} \end{cases}, \quad (9)$$

with W as the weight of the patient (in [kg]) and H as the height of the patient (in [cm]). Once the LBM of the patient is computed, corresponding PID parameters can be calculated as

$$k = 0.081 \cdot c_f, \quad k_i = 0.0055 \cdot c_f, \quad k_d = 45 \cdot c_f, \quad (10)$$

where $c_f = 60\frac{\text{LBM}}{\text{Con}}$ is the scaling factor, with $\text{Con} = 10$ [mg/ml] as the concentration of the used proporol.

Since it is necessary to protect the controller from integral windup, particularly when the infusion rate is nil, a back-calculation Anti-Windup scheme [31] is implemented that resets the integrator dynamically with a time constant $T_t = 60$ [s].

To attenuate the high frequency noise, measured effect is passed through a second-order low-pass measurement filter $F_m(s)$, expressed as:

$$F_m(s) = \frac{1}{(T_m s+1)^2}, \quad (11)$$

where $T_m = 15$ [s] is the time constant. In order to smooth out any step-like changes, the reference signal is also passed through the filter $F_m(s)$.

Propofol will be delivered using an infusion pump, with a lower bound $I_{\min} = 0$ [ml/h] and an upper bound $I_{\max} = 1200$ [ml/h]. The saturation block is used in Figure 2 to represent this limitation.

Finally, for notational compactness, the overall dynamic model of the system can be expressed as

$$\begin{cases} \dot{x}(t) = f(x(t), v(t)) \\ y(t) = h(x(t), v(t)) \end{cases}, \quad (12)$$

where $x(t) \in \mathbb{R}^n$ is the state of the system, $y(t) = \begin{bmatrix} y_1(t) & y_2(t) \end{bmatrix}^T$ is the output of the system with $y_1(t)$ as the

level of hypnosis and $y_2(t) = C_{e,B}(t)$, and $v(t) \in [0,1]$ is the reference level of hypnosis.

As shown in [28, 32], this PID controller provides adequate robustness against the intra- and inter-patient variability observed in the target population. The achieved robust performance without additional constraints is clinically sufficient and achieves sufficiently fast induction of anesthesia. However, high plasma concentrations following induction of anesthesia may occur, and treatment for hypotension is required in some cases [27]. In the following, in order to prevent OD and BPD, we describe constrained control schemes based on the ERG framework, the SPC framework, and the MPC framework.

4. Enforcing Safety with ERG

Clinical anesthesia can be seen as a constrained control problem which includes a number of constraints that must not be violated. Constraints on the amplitude of the propofol infusion rate $I(t)$ are mostly due to hard physical constraints of the system [33] and to safety requirements: 1) the infusion rate can obviously not be negative, and 2) the maximum infusion rate is limited to keep hemodynamics changes bounded. By assuming that Con = 10 [mg/ml], the infusion rate is typically constrained between 0 and 600 [ml/h] [20], i.e.,

$$0 \leq I(t) \leq 600 \text{ [ml/h]}. \tag{13}$$

Safety bounds on the propofol plasma concentration $C_{p,H}(t)$ and effect-site concentration $C_{e,H}(t)$ can be defined using the therapeutic window [34] for propofol. Safety bounds on $C_{p,H}(t)$ and $C_{e,H}(t)$ used in this paper are [35, 36]

$$0 \leq C_{p,H}(t) \leq 10 \text{ [}\mu\text{g/ml]}, \tag{14}$$

$$1.5 \leq C_{e,H}(t) \leq 8 \quad \text{[}\mu\text{g/ml]}. \tag{15}$$

In addition to constraints (14)-(15) that correspond to OD prevention, for safety purposes the patient's BPD also needs to be bounded. As shown in [21], BPD should be limited to be less that 50%, i.e., $E_{o,B}(t) \leq 0.5$. Since (6) is monotonically increasing, its inverse can be used to map the constraint on the BPD to a constraint on $C_{e,B}(t)$, as follows:

$$0 \leq y_2(t) = C_{e,B}(t) \leq \Omega \text{ [}\mu\text{g/ml]}. \tag{16}$$

where Ω is 4.61 for the patients that are in the age range from 20 to 39 years, and is 4.13 for those in the age range from 40 to 59 years.

At this stage, we define the following control problem:

Problem 1. *Consider system* (12) *which is subject to constraints* (13)-(16). *For suitable* $x(0)$ *and* $v(0)$[1], *find an auxiliary reference signal* $v(t)$ *such that constraints* (13)-(16) *are satisfied at all times, and* $v(t)$ *tends to the desired reference.*

As shown in [37, 38], Problem 1 can be solved by manipulating the auxiliary reference $v(t)$ according to the following differential equation:

$$\dot{v}(t) = \kappa \cdot \Delta(t) \cdot \rho(t), \tag{17}$$

where $\kappa > 0$ is a tuning parameter, and $\Delta(t)$ and $\rho(t)$ are the two fundamental components of the ERG scheme, called the Dynamic Safety Margin (DSM) and the Navigation Field (NF), respectively.

The NF represents the direction along a feasible path that leads from the current auxiliary reference v to the desired reference r. Since in this paper the reference is mono-dimensional, we use the most intuitive choice for NF [39], which is:

$$\rho(t) = \frac{r - v(t)}{\max\{|r - v(t)|, \eta\}}, \tag{18}$$

where $\eta > 0$ is a smoothing factor.

The DSM represents a distance between the constraints (13)-(16) and the trajectory of the system (12) that would emanate from the current condition of the system for a constant reference v. In other words, $\Delta(t) \geq 0$ implies that if the current auxiliary reference $v(t)$ is maintained constant, constraints (13)-(16) are satisfied at all times. Moreover, $\Delta(t) > 0$ implies that $v(t)$ can be perturbed without causing constraint violation.

The most intuitive way to compute the DSM is to solve at each time instant the following differential equation:

$$\begin{cases} \dot{\hat{x}}(\tau) = f(\hat{x}(\tau), v(t)) \\ \hat{x}(0) = x(t) \end{cases}, \tag{19}$$

and then to compute $\Delta(t)$ as

$$\Delta(t) = \min_{i \in \{1,\cdots,8\}} \{\Delta_i(t)\}, \tag{20}$$

where $\Delta_i(t)$ is the distance between the i-th constraint[2] and the trajectory of system (19), computed as

$$\Delta_1(t) = \min_{\tau \in [t,\infty)} \{\hat{I}(\tau|t)\}, \tag{21}$$

$$\Delta_2(t) = \min_{\tau \in [t,\infty)} \{600 - \hat{I}(\tau|t)\}, \tag{22}$$

$$\Delta_3(t) = \min_{\tau \in [t,\infty)} \{\hat{C}_{p,H}(\tau|t)\}, \tag{23}$$

$$\Delta_4(t) = \min_{\tau \in [t,\infty)} \{10 - \hat{C}_{p,H}(\tau|t)\}, \tag{24}$$

$$\Delta_5(t) = \min_{\tau \in [t,\infty)} \{\hat{C}_{e,H}(\tau|t) - 1.5\}, \tag{25}$$

$$\Delta_6(t) = \min_{\tau \in [t,\infty)} \{8 - \hat{C}_{e,H}(\tau|t)\}, \tag{26}$$

$$\Delta_7(t) = \min_{\tau \in [t,\infty)} \{\hat{y}_2(\tau|t)\}, \tag{27}$$

$$\Delta_8(t) = \min_{\tau \in [t,\infty)} \{\Omega - \hat{y}_2(\tau|t)\}, \tag{28}$$

[1] By the term "suitable", we mean any set of initial conditions for system (12), which by starting from them, constraints (13)-(16) are never violated (See [37] for more details). Note that in this specific application, for any patient state, $x(0) = 0$ and $v(0) = 0$ is always feasible.

[2] Note that upper and lower bounds in (13)-(16) need to be treated separately, meaning that we have 8 constraints in total.

with $\hat{I}(\tau|t)$, $\hat{C}_{p,H}(\tau|t)$, $\hat{C}_{e,H}(\tau|t)$, and $\hat{y}_2(\tau|t)$ as variables computed via (19) with initial condition $x(t)$.

Clearly, computing $\Delta_i(t),\ i=1,\cdots,8$ at each time instant over an infinite horizon is inapplicable in practice. As shown in [19] and [20], since for a linear system whose state is bounded (which is realistic to consider in our case, as we use the robust PID controller for precompensation) it is easy to characterize the worst case peak time T and to solve (19) up to T, one possible way to tackle the mentioned problem is to approximate the system (12) with a linear system and to provide a closed-form solution for $\Delta_i(t),\ i=1,\cdots,8$.

In particular, first, the system (12) can be approximated with the following linear system[3]

$$\begin{cases} \dot{\tilde{x}}(t) = A\tilde{x}(t) + Bv(t) \\ \tilde{y}(t) = C\tilde{x}(t) \end{cases}, \tag{29}$$

where

$$A = \begin{bmatrix} A_1 & 0 & 0 & 0 & 0 & 0 & 0 \\ B_{21}C1 & A_2 & 0 & 0 & 0 & -B_{22}C_6 & 0 \\ B_3D_{21}C_1 & B_3C_2 & A_3 & 0 & 0 & -B_3D_{21}C_6 & 0 \\ 0 & 0 & B_4C_3 & A_4 & 0 & 0 & 0 \\ 0 & 0 & 0 & B_5C_4 & A_5 & 0 & 0 \\ 0 & 0 & 0 & 0 & B_6C_5 & A_6 & 0 \\ B_7D_{21}C_1 & B_7C_2 & 0 & 0 & 0 & -B_7D_{21}C_6 & A_7 \end{bmatrix}, \tag{30}$$

$$B = \begin{bmatrix} B_1^T & 0 & 0 & 0 & 0 & 0 & 0 \end{bmatrix}^T, \tag{31}$$

$$C = \begin{bmatrix} 0 & 0 & 0 & 0 & C_5 & 0 & 0 \\ 0 & 0 & 0 & 0 & 0 & 0 & C_7 \end{bmatrix}, \tag{32}$$

with (A_1,B_1,C_1,D_1), $(A_2,[B_{21}\quad B_{22}],C_2,[D_{21}\quad D_{22}])$, (A_3,B_3,C_3,D_3), (A_4,B_4,C_4,D_4), (A_5,B_5,C_5,D_5), (A_6,B_6,C_6,D_6), and (A_7,B_7,C_7,D_7) as state-space realization matrices of the set-point filter (11), the control law (8), the PK model (1), the PD model (2), the sensor model (7), the measurement filter (11), and the PK model (4) augmented with the PD model (5), respectively. See [19] and [20] for more details on the linearization procedure.

Then, $\tilde{x}(\tau|t)$ can be computed for $\tau \in [t, t+T]$ as

$$\tilde{x}(\tau|t) = e^{A(\tau-t)}x(t) + \int_t^\tau \left(e^{A(\tau-\sigma)}Bv(t)\right)d\sigma, \tag{33}$$

where T is bigger than the peak time of closed-loop system (29) for all possible initial conditions (see [40] for more details). Finally, $\tilde{I}(\tau|t)$, $\tilde{C}_{p,H}(\tau|t)$, $\tilde{C}_{e,H}(\tau|t)$, and $\tilde{y}(\tau|t)$ can be computed accordingly.

The main advantage of the mentioned formulation is that, being based on the prediction of a linear system, it has a closed-form solution and consequently it is not computationally onerous. However, since possible approximation errors can degenerate the DSM (20) such that resulting DSM might not be valid, the DSM (20) should be modified to guarantee constraints satisfaction at all times. For this purpose, we can restrict the $\Delta_i(t)$s in (21)-(28) as

$$\Delta_i(t) = \Delta_i(t) - \delta_i,\ i=1,\cdots,8, \tag{34}$$

where $\delta_i \geq 0,\ i=1,\cdots,8$ can be interpreted as static safety bounds to take into account the mismatch between (19) and (29). Note that since the PD model (2)-(3) is unknown and we have to use a nominal PD model to calculate the realization matrices (A_4,B_4,C_4,D_4) in (30)-(32), δ_is should also cover possible uncertainties in the PD model of patients.

In order to determine the value of δ_is, let define $e_1(t) \triangleq I(t) - \tilde{I}(t)$, $e_2(t) \triangleq C_{p,H}(t) - \tilde{C}_{p,H}(t)$, $e_3(t) \triangleq C_{e,H}(t) - \tilde{C}_{e,H}(t)$, $e_4(t) \triangleq y_2(t) - \tilde{y}_2(t)$. Then, $\delta_i,\ i=1,\cdots,8$ can be determined as

$$\delta_1 = \delta_2 = \max_{n\in\{1,\cdots,N\}} \sup_{t\geq 0} |e_1(t)|, \tag{35}$$

$$\delta_3 = \delta_4 = \max_{n\in\{1,\cdots,N\}} \sup_{t\geq 0} |e_2(t)|, \tag{36}$$

$$\delta_5 = \delta_6 = \max_{n\in\{1,\cdots,N\}} \sup_{t\geq 0} |e_3(t)|, \tag{37}$$

$$\delta_7 = \delta_8 = \max_{n\in\{1,\cdots,N\}} \sup_{t\geq 0} |e_4(t)|, \tag{38}$$

where N is the number of patients. Note that in $e_i(t),\ i=1,\cdots,4$, tilded variables are computed through (33) where matrices A, B, and C are built using a nominal PD model, whereas non-tilded variables are computed using actual PKPD model (1)-(6).

In this paper, in order to determine the value of $\delta_i,\ i=1,\cdots,8$, we consider 44 patient models identified from clinical data as described in [24]. As discussed in [17, 41], patient age can be used as a criterion to reduce the inter-individual variability of the PKPD models. Hence, a 10-years bracket is selected and the 44 patients are subdivided into four age groups, as Group 1: 18-29 years, Group 2: 30-39 years, Group 3: 40-49 years, and Group 4: 50-60 years. Then, a nominal model for each age group is identified using the averaging method [17]. In order to make sure that the method is robust against larger uncertainties that may exist in different sets of patients, 1000 "virtual patients" for each age group have been generated using the method presented in [20]. More precisely, we have then generated the "virtual patients" by randomly selecting the parameter p in the range $p-1.1\phi$ and $p+1.1\phi$, where ϕ is the maximal distance between the nominal value of the parameter p and the actual values of the same parameter. Finally, a Monte Carlo simulation study was carried out by generating a random step-wise reference signal with random number of steps, durations, and levels. Simulation results are shown in Figure 3, and obtained values for $\delta_i,\ i=1,\cdots,8$ are 0.35, 0.35, 1.2, 1.2, 1.2, 1.2, 0.9, and 0.9, respectively.

Note that, in this paper, we use the PK model proposed by Schüttler and Ihmsen [25], as the parameters of the 44 patients are identified using this model [24]. However, since the PK model proposed by Schnider *et al.* [26] is commonly used in clinical target-controller infusion systems to report the plasma

[3] The control law (8) is implemented as a two-input-one-output linear time-invariant system. To compute (A_4,B_4,C_4,D_4), the time-delay operator in (2) is approximated by Padè approximant.

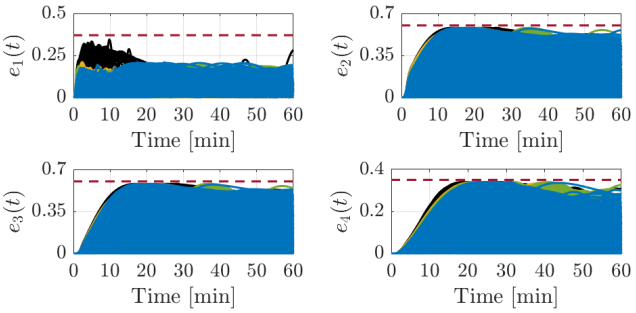

Figure 3: Illustration of determining safety bounds δ_i, $i = 1, \cdots, 8$; black lines: Group 1, yellow lines: Group 2, green lines: Group 3, blue lines: Group 4, and red dashed lines: obtained values for δ_is.

and effect-site concentrations [42], we employ the PK model given in [26] to study the constraints on $C_{p,H}(t)$ and $C_{e,H}(t)$, i.e., constraints (14)-(15). It should be remarked that to study the constraints (14)-(15), as reported in [26], PD model (2) is identical for all patients with $T_d = 0$ [s] and $k_{d,H} = 0.456$ [min^{-1}], i.e., the constraints are known.

In summary, the ERG-based constraint enforcement unit is implemented as (17), where $\rho(t)$ is computed through (18), and $\Delta(t)$ is computed through (20) with $\Delta_i(t)$ as in (34). It should be remarked that the main advantage of the proposed method is its simplicity and low computational complexity, which makes it applicable for real-time drug delivery purposes.

In the following remark, two modifications to the basic ERG are presented, which are used in this paper to ensure an extra level of safety.

Remark 1. *As shown in [43], in the presence of a bounded external disturbance $d(t)$ (i.e., $\sup_{t\geq 0}\|d(t)\| < \infty$), the $\Delta_i(t)$ needs to be updated as*

$$\Delta_i(t) = \Delta_i(t) - \delta_i - \delta_i^d, \tag{39}$$

where δ_i^d should cover uncertainty due to the external disturbance. The value of δ_i^d can be computed via a Monte Carlo simulation study by assuming the upper-bound of the disturbance $d(t)$.

Remark 2. *The ERG guarantees constraints satisfaction at all times. In other words, ERG guarantees that the states of the system remain within a safe region in which $\Delta \geq 0$. In some cases (e.g., the scenario studied in Subsection 7.3) an unwanted deviation in the trajectory of the system can happen due to unmodeled uncertainty or unforeseen external disturbance exceeding the design guaranteed bounds. This deviation may cause the states of the system to enter the unsafe region in which $\Delta < 0$. One intuitive way to cope with this problem is to modify the ERG scheme given in* (17) *as*

$$\begin{cases} \dot{v} = \kappa \cdot \Delta \cdot \rho & \Delta \geq 0 \\ \dot{v} = \bar{\kappa} \cdot \nabla_v \Delta & \Delta < 0 \end{cases}, \tag{40}$$

where $\bar{\kappa}$ is a design parameter, and $\nabla_v \Delta$ denotes the gradient of Δ with respect to v. This new control scheme is so that when the states of the system are in the safe region, the auxiliary reference $v(t)$ changes as the basic ERG formulation (17)*, but, when the states enter the unsafe region (i.e., $\Delta < 0$), the auxiliary reference $v(t)$ changes in accordance with the gradient of Δ. More precisely, when $\Delta < 0$, the auxiliary reference changes such that the value of the dynamic safety margin Δ increases, and consequently states of the system reenter the safe region.*

5. Enforcing Safety with SPC

SPC employs Formal Methods [44] to approximate the viability kernel. For a dynamic system X with $\mathscr{K}$ and $\mathscr{I}$ as convex-compact sets of safety constraints on its states and inputs, respectively, the viability kernel $Viab(\mathscr{K},\mathscr{I},X)_{[t,\tau]}$ is a set of states at time t starting from which there exists an input within $\mathscr{I}$ that maintains the states of X within $\mathscr{K}$ for all time in $[t,\tau]$, i.e.,[4]:

$$Viab(\mathscr{K},\mathscr{I},X)_{[t,\tau]} = \{x(0) \in \mathscr{K} \mid \exists I(\cdot) : [t,\tau] \to \mathscr{I}, \text{ such that } x(t) = x(0) \;\&\; x(t') \in \mathscr{K},\ \forall t' \in [t,\tau]\}. \tag{41}$$

If the viability kernel is empty, there exists no feasible control solution for the given constrained control problem. On the other hand, if the viability kernel is not empty, SPC synthesizes a constrained controller (called safety-preserving) to find an appropriate input for the constrained control problem. This controller is guaranteed to maintain safety as the feasibility of the constraints is demonstrated through the viability kernel approximation. Several safety-preserving controllers have been proposed in the literature (e.g. [48, 49, 50, 51, 52]).

For the sake of comparison with MPC and ERG, we employ the safety-preserving controller presented in [22] which is formulated to avoid drug overdosing and hypotension in closed-loop anesthesia. In this scheme, the closed-loop control input is calculated as follows:

$$I(t) = (1-\beta_\alpha) I_{pr}(t) + \beta_\alpha I_{sp}(t). \tag{42}$$

where I_{pr} is a performance control input which is calculated by a closed-loop controller to satisfy performance criteria. In the case of the closed-loop anesthesia problem, I_{pr} is calculated by the PID controller as discussed previously. In (42), I_{sp} refers to a safety-preserving control action which is guaranteed to maintain the states within the safe region, and β_α is determined as

$$\beta_\alpha = \begin{cases} 0 & , \quad \alpha < \vartheta(x(t)) \\ \dfrac{\alpha - \vartheta(x(t))}{\alpha} & , \quad 0 < \vartheta(x(t)) \leq \alpha \\ 1 & , \quad \vartheta(x(t)) \leq 0 \end{cases}, \tag{43}$$

where $\alpha \in [0,1)$ is a design variable and $\vartheta(x(t))$ is a signed distance between the state vector $x(t)$ and boundaries of $Viab(\mathscr{K},\mathscr{I},X)_{[t,\tau]}$ [52]. The distance is negative if $x(t) \notin Viab(\mathscr{K},\mathscr{I},X)_{[t,\tau]}$. Accordingly, as the states approach the

[4] For different methods of viability kernel approximation, see [45, 46, 47]

boundaries of $Viab(\mathscr{K},\mathscr{I},X)_{[t,\tau]}$ the safety-preserving controller contributes more and pushes the states inside the safe region.

To calculate the safety-preserving control input in (42), we employ the safety-preserving control policy formulated by [53]. Accordingly, assuming the constraint set is compact, convex and h-continuous[5], the following control policy is safety-preserving:

$$I_{sp}(t) = \arg\min_{I(t)} \{\langle l^{\circ}(t), BI(t)\rangle | I(t) \in \mathscr{I}\}, \tag{44}$$

where

$$l^{\circ}(t) = \arg\max_{l} \{\langle l, x(t)\rangle - \theta(l, Viab(\mathscr{K},\mathscr{I},X)_{[t,\tau]}) |\ \|l\| \leq 1\}, \tag{45}$$

with $\langle\cdot,\cdot\rangle$ as the inner product of two vectors, and $\theta(l, Viab(\mathscr{K},\mathscr{I},X)_{[t,\tau]})$ as the support function of $Viab(\mathscr{K},\mathscr{I},X)_{[t,\tau]}$ in direction l.

The details of using the above-mentioned safety-preserving control policy in closed-loop anesthesia can be found in [22]. We also refer the readers to [22] for the details of the approximated viability kernel for the 44-patient model set.

6. Enforcing Safety with MPC

The MPC scheme in this paper was designed specifically for a comparison with ERG and SPC. The design objective is to achieve an unconstrained closed-loop response similar to the response with the PID controller described above, for the population of 44 virtual patients as presented by [24]. It was not designed to optimize performance in any way, other than to achieve similar performance as the PID controller. To achieve this, the MPC scheme was manually tuned.

The MPC scheme utilized in this paper is based on the SISO propofol controller detailed in [23]. Note that several MPC schemes have been presented in the literature, e.g., [12, 14, 54, 55, 56, 57, 58]. These schemes cannot be used directly to compare constrained control performance, as results are confounded by design choices, variability in the models considered, and the reported performance metrics. We therefore design an MPC controller with the objective to achieve comparable performance to the PID controller described in Section 3, for the model set described in Section 2.

The controller includes the nominal model detailed in [23], whose realization matrices are (A_p, B_p, C_p, D_p). To achieve similar unconstrained closed-loop responses as the PID controller, the delay of this nominal model is reduced to one time sample, limiting the internal delays in the MPC controller. The model is augmented with the sensor model and integral action is included by using optimizing the change in input $\Delta u_p(t)$. The augmented model of the controller also includes a step disturbance model and feedback is introduced using unity state feedback on this disturbance state (see [23] for more details).

[5] See [53] for the definition of h-continuity.

With a discrete state-space description of the model relating $\Delta u_p(t)$ to the the level of hypnosis given by (A_p, B_p, C_p, D_p), sampled at 5 seconds, the prediction model is given by:

$$\begin{cases} \hat{x}(t+1) = A\hat{x}(t) + B\Delta u_P(t) \\ \hat{y}(t) = C\hat{x}(t) \end{cases}, \tag{46}$$

where $\hat{y}(t)$ represents the predicted level of hypnosis, $\hat{x}(t) = \left[x_p(t)\ \hat{d}(t)\right]^T$, with x_p corresponding to the states of the propofol model, and $\hat{d}$ is the estimation of the disturbance which represents the effect of model uncertainties, and

$$A = \begin{bmatrix} A_p & 0 \\ 0 & 1 \end{bmatrix},\ B = \begin{bmatrix} B_p \\ 0 \end{bmatrix},\ C = \begin{bmatrix} C_p & 1 \end{bmatrix}. \tag{47}$$

The disturbance state (i.e., model uncertainties) is estimated using a Luenberger observer with $L = [\mathbf{0}\ \mathbf{1}]$, and as seen in (46), it is assumed to be constant during prediction horizon.

The standard MPC optimization criterion is minimized at each time step, using weight matrices for the prediction error and the control effort, as follows:

$$\begin{aligned} J_E(t) = &\sum_{i=1}^{H_p} \left(r(t+i) - \hat{y}(t+i|t)\right)^2 q_p(i) \\ &+ \sum_{k=1}^{H_c} \left(\Delta u_P(t+k-1|t)\right)^2 r_p(k), \end{aligned} \tag{48}$$

where H_p is the prediction horizon, H_c is the control horizon, and the weights are given by $q_p(i)$ and $r_p(i)$. Note that $\Delta u_P(t+k|t) = 0, \forall k > H_p$.

The tuning structure proposed in [23] was used, where $r_p(k) = 10R$ for $k = 1$, $r_p(k) = 500R$ for $k > 1$, $q_p(i) = 0$ for $i = 1$, $q_p(i) = Q$ for $i \in [2, Q_{cut}]$, and $q_p(i) = 100Q$ for $i > Q_{cut}$. The horizon lengths H_p and H_c, and the tuning parameters Q, R, and Q_{cut}, were determined using a grid search. The ten tuning combinations with the 10 lowest mean square errors compared to the unconstrained PID implementation (for the complete population of 44 virtual patients) were selected and the responses were visually inspected. Finally, the controller that best represented the overshoot and Induction Time (IT)[6] achieved by the PID controller was selected. The tuning parameters of this controller are $H_p = 240$, $H_c = 3$, $Q = 1000$, $R = 1$, and $Q_{cut} = 80$.

Since the constraints are based on different PKPD models than the nominal model, an additional state space model is introduced for the constraints. The constrained MPC scheme optimizes the resulting constrained quadratic program at each time step, i.e., it minimizes the cost function (48) subject to constraints (13)-(16).

7. Results and Discussion

To compare the performance of the ERG, SPC, and MPC schemes, we consider the set of 44 patient models identified

[6] Induction Time (IT) is defined as the time taken by $y_1(t)$ to reach 0.4 and stays above it for more than 30 [sec] [22].

in [24], and we simulate the clinical scenarios, i.e.: 1) normal mode as used in [22], and 2) stimulation and 3) low clearance as proposed in [15]. The simulations are run using the values $T = 50$ [min] and $r = 0.5$, with the ERG parameters $\kappa = 1$, $\eta = 0.01$ and $\alpha = 0.2$.

7.1. Scenario 1: Normal Mode (Constraints on C_p,C_e and BPD)

In this scenario, all 44 PKPD patient models with the structure described in equation (1)-(6) are considered. For the sake of simplicity and convenience, the DOH is defined as follows

$$\mathrm{DOH}(t) \triangleq 100 \cdot (1 - y_1(t)), \tag{49}$$

where maximum and minimum hypnotic effects correspond to $\mathrm{DOH}(t) = 0$ and $\mathrm{DOH}(t) = 100$, respectively. Also, BPD is defined as

$$\mathrm{BPD}(t) \triangleq 100 \cdot E_{o,B}. \tag{50}$$

Simulation results are shown in Figure 4. All schemes ensure that the constraints are satisfied, with the DOH converging to the reference signal. Table 1 compares performance of the ERG, SPC, and MPC schemes with respect to indices: 1) IT, 2) Rise Time (RT), which is defined as the time taken by DOH to change from 95 [%] to 55 [%] [28], 3) Settling Time (ST), which is defined as the time taken by DOH to enter the interval [40,60] [%] and stay there [17], 4) Overshoot (OS), which represents the maximum peak value of DOH measured from 50 [%] [28], and 5) Used Drug for Induction (UDI), defined as the total amount of drug used during induction phase [20].

The time-profile of the auxiliary reference signal $v(t)$ in the ERG framework, Figure 5, illustrates how ERG manipulates the auxiliary reference $v(t)$ only when the manipulation does not lead to constraint violation. In simple terms, by using the ERG, instead of applying the desired DOH instantly, we apply the auxiliary reference $v(t)$ that automatically converges to the desired DOH so that OD prevention and BPD prevention are guaranteed at all times.

The transient responses of the DOH to satisfy the constraints are different for the three methods. ERG exhibits a slower response to induction of anesthesia with smooth profiles (see Figure 4), with a maximal induction time of over 30 minutes (Table 1). This slow induction would be clinically unacceptable. The maximal induction times achieved with SPC and MPC are 11.6 and 7.2 minutes, respectively, which would also introduce clinical challenges, as it could delay the anesthesiologists ability to secure the airway and it could delay the start of surgery. However, IT below 5 minutes may not be achievable with these constraints.

For some patients the achieved DOH shows an increase to > 60 when the constraints are active in SPC and MPC, after an initial decrease to below 60 and completed induction of anesthesia. This behaviour could be clinically undesired as DOH > 60 may risk inter-operative awareness [28], and DOH > 60 at the start of the procedure can be particularly problematic and delay surgery. Note that the corresponding DOH in the ERG scheme remains > 60, where the constraints led to longer induction times (IT). Settling times (ST) are more comparable between methods. This may indicate that a faster settling time may not be achievable with these constraints.

Table 1: Comparing Performance Indices.

Index	ERG	SPC	MPC
IT [min]			
mean±SD	7.09±6.28	5.28±1.70	4.30±0.80
[min, max]	[3.69,30.92]	[3.47,11.60]	[3.17,7.17]
RT [min]			
mean±SD	7.91±10.44	8.42±11.84	5.06±7.45
[min, max]	[2.17,43.16]	[2.30,49.53]	[1.75,39.58]
ST [min]			
mean±SD	9.83±6.44	9.85±6.88	7.477±5.52
[min, max]	[3.88,30.91]	[3.95,27.07]	[3.25,22.50]
OS [%]			
mean±SD	13.99±10.49	14.32±8.51	14.48±7.34
[min, max]	[0,30.26]	[0,30.94]	[0,26.67]
UDI [ml]			
mean±SD	19.19±11.28	17.22±5.60	15.82±3.60
[min, max]	[8.97,58.38]	[8.88,33.37]	[9.16,23.94]

MPC introduced short-period high-frequency oscillations in the infusion rate for some patients when the constraints were reached, while the ERG and the SPC provide smooth injection overall (see Figure 4). MPC achieves faster induction, with similar overshoot and less drug use than ERG and SPC. Note that the unconstrained controller in the MPC implementation is similar but not equivalent to the PID controller used in the SPC and ERG schemes.

7.2. Scenario 2: Stimulation

In this scenario, closed-loop anesthesia is simulated for the patient #35. It is assumed that the disturbance shown in Figure 6 is applied to the system, which results in reaching the upper bound of the effect-site concentration $C_{e,H}$.

Simulation results are shown in Figure 7. Note that for this scenario the ERG scheme is modified to be robust against the external disturbance by adding an extra static safety margin as discussed in Remark 1. The ERG solution is conservative compared to the SPC and MPC solution: drug infusion is lower and consequently induction of anesthesia is slower using the ERG scheme compared to the SPC scheme. Note that the constraint is not reached in the MPC solution.

When the constraint is approached in the SPC scheme, the control policy that drives the states away from the bound is more aggressive than the MPC or ERG policy, and the input saturates at the lower limit (zero infusion). The system states are forced well away from the bounds as shown in the predicted effect site concentration in Figure 7.

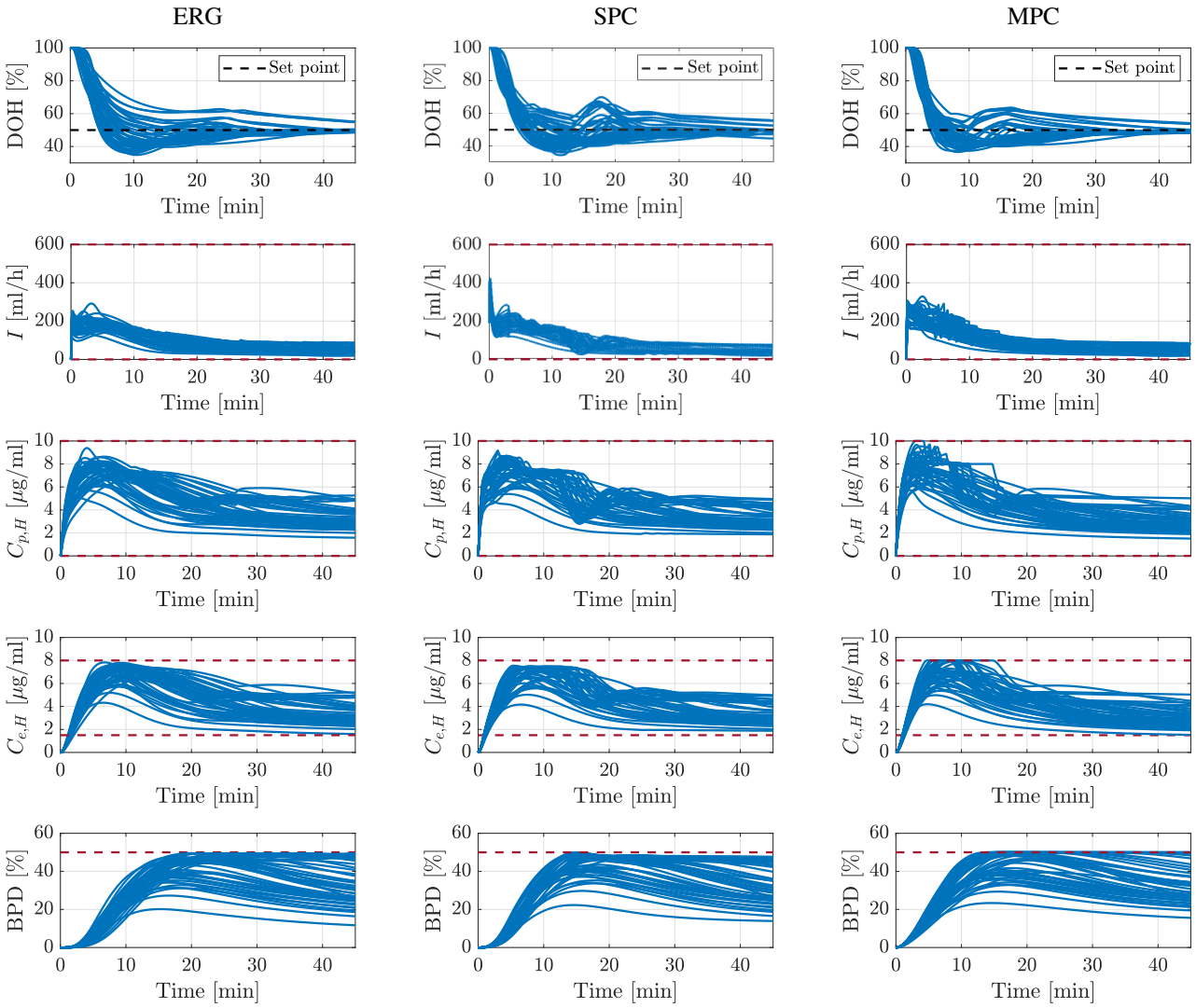

Figure 4: The simulated responses of the 44 patients; left column: results with ERG, middle column: results with SPC, and right column: results with MPC.

7.3. Scenario 3: Low Clearance

To simulate reduced clearance, the non-linear model of patient #15 is multiplied by

$$G_2(s) = 1 + \frac{0.8}{(700s+1)(800s+1)^2}, \tag{51}$$

which increases the gain at low frequency, and consequently, due to the reduced clearance, the lower bound of $C_{e,H}$ is reached. Furthermore, the disturbance shown in Figure 6 is applied to the system.

This scenario includes multiple challenges. The model with reduced clearance is significantly different at low frequencies compared to any nominal model used for controller design for the population. Furthermore, even though the control action is limited due to an active lower bound, the controller needs to be responsive to the increase in measured DOH to provide sufficient anesthesia in the presence of the disturbance.

Simulation results are shown in Figure 8. Note that for this scenario the ERG scheme is modified as discussed in Remark

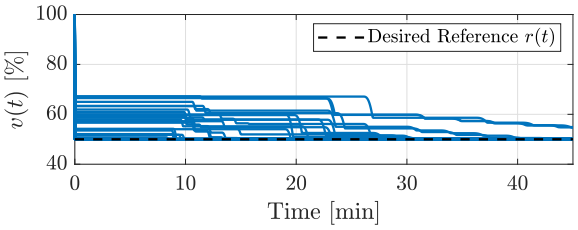

Figure 5: Time profile of the auxiliary reference signal $v(t)$.

2. The ERG scheme (based on the uncertain closed-loop system) is conservative for this patient, i.e., induction of anesthesia is slower than the unconstrained PID controller while the predicted effect site concentration remains well clear of the bound. This slow induction and prolonged DOH near 60 is clinically undesired. Once the lower bound is reached, all three methods maintain the system within bounds, while the unconstrained system would not meet the safety constraints.

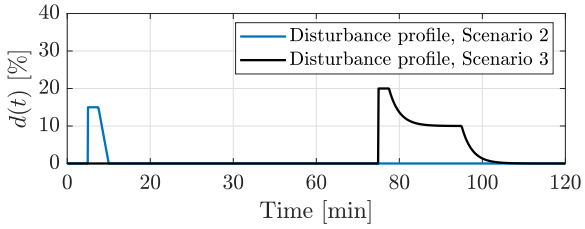

Figure 6: Disturbance profile used in Scenarios 2 and 3.

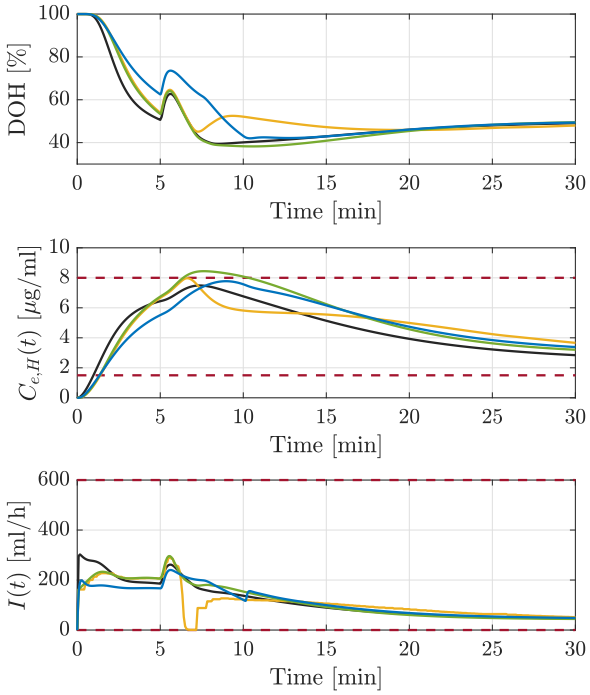

Figure 7: Simulation results for Scenario 2; blue line: ERG, black line: MPC, yellow line: SPC, and green line: unconstrained control.

Following the disturbance after 70 minutes, the SPC controller allows for a rapid increase in drug infusion that can compensate for the increased stimulation. The drug infusion shows high frequency oscillation when the bound is reached. The MPC scheme leads to a lower drug infusion in response to stimulation than the SPC controller, likely due to the model-patient mismatch and consequent inaccurate predictions used for optimization. The ERG scheme overdoses this patient following the disturbance, with infusion rates that are significantly higher than the unconstrained solution. When the lower bound is reached, the ERG scheme adjusts the reference signal to reduce the drug infusion and to remain within the bounds. When the disturbance increases the measured DOH value, this lowered reference to the same PID controller leads to higher infusion rates and consequent overdosing.

8. Concluding Remarks

This paper investigates application of different constrained control schemes in closed-loop anesthesia to control the DOH. To ensure patient safety, operational constraints are formulated

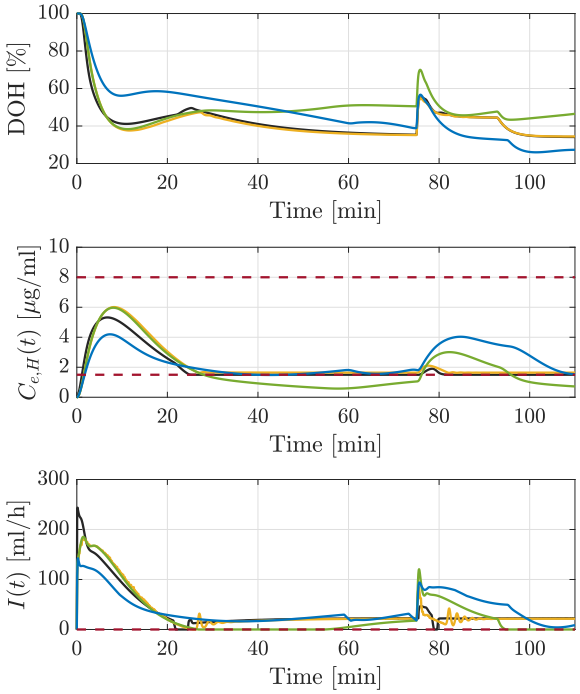

Figure 8: Simulation results for Scenario 3; blue line: ERG, black line: MPC, yellow line: SPC, and green line: unconstrained control.

to avoid OD and BPD. A constrained control method is then used to enforce constraints satisfaction. In this paper, three methods were studied: ERG, SPC, and MPC. The schemes were verified according to three clinical scenarios: 1) normal mode, 2) stimulation, and 3) low clearance.

In this application, with the considered constraints, a robust controller is required to control the uncertain system (patient model). In this work, robustness for the unconstrained system is ensured using a robust PID controller for SPC and ERG, and an MPC controller designed to achieve similar unconstrained performance, and therefore similar robustness merits. The constraints are known, deterministic and do not introduce any uncertainty. The addition of the constraints does not introduce conservatism to the solution of MPC and SPC, as the constraints are known and not affected by the uncertainty in the closed-loop. The ERG scheme uses the uncertain closed-loop system to ensure constraints satisfaction. The solution is therefore conservative, manifested in slower induction of anesthesia. However, ERG guarantees safety even in the presence of a large (unrealistic) model uncertainty.

All three methods maintained the system considered within the constraints, but the transient responses in specific clinical scenarios were significantly different. Similar to model-based anti-windup scheme considered in [15], MPC may not behave as designed (for the nominal model) in the cases where the constraints are most likely to be met, i.e., where the patient-model mismatch is large. An advantage of ERG and SPC is that these schemes can be added to any (precompensating) controller. ERG might be advantageous in terms of transparency and interpretability by clinicians. Further research may be re-

quired for an ERG controller that provides clinically desired behaviour in challenging clinical scenarios.

The MPC controller was designed to be similar to the robust PID controller considered. However, the resulting (unconstrained) controller was not the exact same. MPC outperformed both ERG and SPC in terms of speed of induction of anesthesia in scenario 1, without increasing the overshoot. In scenario 2, the MPC controller achieved faster induction of anesthesia than the PID controller, while the constraint was not reached. Designing a precompensating controller that optimizes the performance while limiting the number of cases and scenarios where the constraints are reached may improve overall constrained system performance. However, constrained controllers are still required to ensure patients' safety by preventing constraint violations.

References

[1] N. Liu, T. Chazot, A. Genty, A. Landais, A. Restoux, K. McGee, P. Laloë, B. Trillat, L. Barvais, M. Fischler, Titration of propofol for anesthetic induction and maintenance guided by the bispectral index: Closed-loop versus manual controla prospective, randomized, multicenter study, Anesthesiology 104 (4) (2006) 686–695.

[2] G. D. Puri, B. Kumar, J. Aveek, Closed-loop anaesthesia delivery system (CLADS (TM)) using bispectral index: a performance assessment study, Anaesthesia and Intensive Care 35 (3) (2007) 357.

[3] N. Liu, M. Le Guen, F. Benabbes-Lambert, T. Chazot, B. Trillat, D. I. Sessler, M. Fischler, Feasibility of closed-loop titration of propofol and remifentanil guided by the spectral m-entropy monitor, Anesthesiology 116 (2) (2012) 286–295.

[4] G. A. Dumont, J. M. Ansermino, Closed-loop control of anesthesia: a primer for anesthesiologists, Anesthesia & Analgesia 117 (5) (2013) 1130–1138.

[5] N. West, G. A. Dumont, K. van Heusden, C. L. Petersen, S. Khosravi, K. Soltesz, A. Umedaly, E. Reimer, J. M. Ansermino, Robust closed-loop control of induction and maintenance of propofol anesthesia in children, Pediatric Anesthesia 23 (8) (2013) 712–719.

[6] E. Brogi, S. Cyr, R. Kazan, F. Giunta, T. M. Hemmerling, Clinical performance and safety of closed-loop systems: A systematic review and meta-analysis of randomized controlled trials, Anesthesia & Analgesia 124 (2) (2017) 446–455.

[7] N. West, K. van Heusden, M. Görges, S. Brodie, A. Rollinson, C. L. Petersen, G. A. Dumont, J. M. Ansermino, R. N. Merchant, Design and evaluation of a closed-loop anesthesia system with robust control and safety system, Anesthesia & Analgesia 127 (4) (2018) 883–894.

[8] M. Hosseinzadeh, Robust control applications in biomedical engineering: Control of depth of hypnosis, in: A. T. Azar (Ed.), Control Applications for Biomedical Engineering Systems, Academic Press, 2020, Ch. 4, pp. 89–125.

[9] T. Kazama, K. Ikeda, K. Morita, M. Kikura, T. Ikeda, T. Kurita, Y. Nakajima, Comparison of the effect-site k(eo)s of propofol for blood pressure and eeg bispectral index in elderly and younger patients, Anesthesiology 90 (6) (1999) 1517–1527.

[10] N. West, K. van Heusden, M. Gorges, C. L. Petersen, A. Umedaly, G. A. Dumont, J. M. Ansermino, R. N. Merchan, Blood pressure changes during closed-loop control of anesthesia, in: Proc. Canadian Anesthesiologists Society Annual Meeting, St. John's, NL, Canada, 2014.

[11] A. Gentilini, C. W. Frei, A. H. Glattfedler, M. Morari, T. Sieber, R. Wymann, T. W. Schnider, A. M. Zbinden, Multitasked closed-loop control in anesthesia, IEEE Eng. Med. Biol. 20 (1) (2001) 39–53.

[12] R. R. Rao, B. Aufderheide, B. W. Bequette, Experimental studies on multiple-model predictive control for automated regulation of hemodynamic variables, IEEE Trans. Biomed. Eng. 50 (3) (2003) 277–288.

[13] R. R. Rao, B. Aufderheide, B. W. Bequette, Control for automated regulation of hemodynamic variables, IEEE Trans. Biomed. Eng. 50 (3) (2003) 277–288.

[14] Y. Sawaguchi, E. Furutani, G. Shirakami, M. Araki, K. Fukuda, A model-predictive hypnosis control system under total intravenous anesthesia, IEEE Trans. Biomed. Eng. 55 (3) (2008) 874–887.

[15] K. van Heusden, N. West, A. Umedaly, J. M. Ansermino, R. N. Merchant, G. A. Dumont, Safety, constraints and anti-windup in closed-loop anesthesia, IFAC Proceedings Volumes 47 (3) (2014) 6569–6574.

[16] M. Yousefi, K. van Heusden, I. M. Mitchell, J. M. Ansermino, G. A. Dumont, A formally-verified safety system for closed-loop anesthesia, IFAC-PapersOnLine 50 (1) (2017) 4424–4429.

[17] N. Sadati, M. Hosseinzadeh, G. A. Dumont, Multi-model robust control of depth of hypnosis, Biomed. Signal Process. Control 40 (2018) 443–453.

[18] M. Hosseinzadeh, E. Garone, Constrained control in closed-loop anesthesia, in: Proc. 38th Benelux Meeting on Systems and Control, Lommel, Belgium, 2019, p. 135.

[19] M. Hosseinzadeh, K. van Heusden, G. A. Dumont, E. Garone, An explicit reference governor scheme for closed-loop anesthesia, in: Proc. 18th Eur. Control Conf., Naples, Italy, 2019, pp. 1294–1299.

[20] M. Hosseinzadeh, G. A. Dumont, E. Garone, Constrained control of depth of hypnosis during induction phase, IEEE Trans. Control Syst. Technol. (2019).

[21] S. Khosravi, Constrained model predictive control of hypnosis, Ph.D. thesis, Univeristy of British Columbia (2008).

[22] M. Yousefi, K. van Heusden, N. West, I. M. Mitchell, J. M. Ansermino, G. A. Dumont, A formalized safety system for closed-loop anesthesia with pharmacokinetic and pharmacodynamic constraints, Control Eng. Pract. (2018).

[23] N. Eskandari, K. van Heusden, G. A. Dumont, Extended habituating model predictive control of propofol and remifentanil anesthesia, Biomed. Signal Process. Control 55 (Jan. 2020).

[24] S. Bibian, G. A. Dumont, M. Huzmezan, C. R. Ries, Patient variability and uncertainty quantification in clinical anaesthesia: part I, PKPD modelling and identification, in: Proc. 6th IFAC Symp. Modelling and Control in Biomedical Systems, Reims, France, 2006.

[25] J. Schüttler, H. Ihmsen, Population pharmacokinetics of propofol: a multicenter study, Anesthesiology 92 (2000) 727–738.

[26] T. W. Schnider, C. F. Minto, P. L. Gambus, C. Andresen, D. B. Goodale, S. L. Shafer, E. J. Youngs, The influence of method of administration and covariates on the pharmacokinetics of propofol in adult volunteers, Anesthesiology 88 (5) (1998) 1170–1182.

[27] N. West, K. van Heusden, M. Gorges, S. Brodie, A. Rollinson, C. L. Petersen, G. A. Dumont, J. M. Ansermino, R. N. Merchant, Design and evaluation of a closed-loop anesthesia system with robust control and safety system, Anesthesia & Analgesia 127 (4) (2018) 883–894.

[28] G. A. Dumont, A. Martinez, J. M. Ansermino, Robust control of depth of anesthesia, Int. J. Adapt. Control Signal Process. 23 (5) (2009) 435–454.

[29] T. Zikov, S. Bibian, G. A. Dumont, M. Huzmezan, C. R. Ries, Quantifying cortical activity during general anesthesia using wavelet analysis, IEEE Trans. Biomed. Eng. 53 (4) (2006) 617–632.

[30] R. Hume, Prediction of lean body mass from height and weight, J. Clin. Pathol. 19 (1966) 389–391.

[31] K. J. Aström, T. Hägglund, Advanced PID Control, ISA- The Instrumentation, Systems, and Automation Society,, 2006.

[32] G. A. Dumont, N. Liu, C. Petersen, T. Chazot, M. Fischler, J. M. Ansermino, Closed-loop administration of propofol guided by the neurosense: Clinical evaluation using robust proportional-integral-derivative design, in: Proc. American Society of Anesthesiologists Annual Meeting, Chicago, Illinois, USA, 2011.

[33] M. Hosseinzadeh, M. J. Yazdanpanah, Robust adaptive passivity-based control of open-loop unstable affine nonlinear systems subject to actuator saturation, IET Control Theory A. 11 (16) (2017) 2731–2742.

[34] J. Vuyk, M. J. Mertens, E. Olofsen, A. G. Burm, J. G. Bovill, Propofol anesthesia and rational opioid selection: determination of optimal EC50-EC95 propofol-opioid concentrations that assure adequate anesthesia and a rapid return of consciousness, Anesthesiology 87 (6) (1997) 1549–1563.

[35] G. E. van Poucke, L. J. Bravo, S. L. Shafer, Target controlled infusions: targeting the effect site while limiting peak plasma concentration, IEEE Trans. Biomed. Eng. 51 (11) (1004) 1869–1875.

[36] B. Yaghooti, M. Hosseinzadeh, B. Sinopoli, Constrained control of semi-linear fractional-order systems: Application in drug delivery systems, in: Proc. 4th IEEE Conf. Control Technology and Applications, Montréal, Canada, 2020.

[37] M. M. Nicotra, E. Garone, The explicit reference governor: A general framework for the closed-form control of constrained nonlinear systems, IEEE Control Syst. Mag. 38 (4) (2018) 89–107.
[38] M. Hosseinzadeh, E. Garone, An explicit reference governor for the intersection of concave constraints, IEEE Trans. Autom. Control 65 (1) (2020) 1–11.
[39] M. Hosseinzadeh, A. Cotorruelo, D. Limon, E. Garone, Constrained control of linear systems subject to combinations of intersections and unions of concave constraints, IEEE Control Syst. Lett. 3 (3) (2019) 571–576.
[40] E. Garone, I. Kolmanovsky, S. D. Cairano, Reference and command governors for systems with constraints: a survey on theory and applications, Automatica 75 (2016) 306–328.
[41] T. W. Schnider, C. F. Minto, S. L. Shafer, P. L. Gambus, C. Andresen, D. B. Goodale, E. J. Youngs, The influence of age on propofol pharmacodynamics, Anesthesiology 90 (6) (1999) 1502–1516.
[42] A. Absalom, J. Glen, G. J. Zwart, T. Schnider, M. M. R. Struys, Target-controlled infusion: A mature technology, Anesthesia & Analgesia 122 (1) (2016) 70–78.
[43] M. M. Nicotra, Constrained control of nonlinear systems: The explicit reference governor and its application to unmanned aerial vehicles, Ph.D. thesis, Université Libre de Bruxelles & Université di Bologna (2016).
[44] E. Clarke, The birth of model checking, in: 25 Years of Model Checking, Springer, 2008, pp. 1–26.
[45] S. Kaynama, J. Maidens, M. Oishi, I. M. Mitchell, G. A. Dumont, Computing the viability kernel using maximal reachable sets, in: Proc. 15th ACM int. conf. Hybrid Systems: Computation and Control, ACM, 2012, pp. 55–64.
[46] J. N. Maidens, S. Kaynama, I. M. Mitchell, M. K. Oishi, G. A. Dumont, Lagrangian methods for approximating the viability kernel in high-dimensional systems, Automatica 49 (7) (2013) 2017–2029.
[47] K. Margellos, J. Lygeros, Viable set computation for hybrid systems, Nonlinear Anal. Hybrid Syst. 10 (2013) 45–62.
[48] K. Margellos, J. Lygeros, Hamilton-jacobi formulation for reach-avoid differential games, IEEE Trans. Autom. Control 56 (8) (2011) 1849–1861.
[49] J. Lygeros, C. Tomlin, S. Sastry, Controllers for reachability specifications for hybrid systems, Automatica 35 (3) (1999) 349–370.
[50] J. Lygeros, On reachability and minimum cost optimal control, Automatica 40 (6) (2004) 917–927.
[51] I. M. Mitchell, A. M. Bayen, C. J. Tomlin, A time-dependent hamilton-jacobi formulation of reachable sets for continuous dynamic games, IEEE Trans. Autom. Control 50 (7) (2005) 947–957.
[52] S. Kaynama, I. M. Mitchell, M. Oishi, G. A. Dumont, Scalable safety-preserving robust control synthesis for continuous-time linear systems, IEEE Trans. Autom. Control 60 (11) (2015) 3065–3070.
[53] A. Kurzhanski, I. Vályi, Ellipsoidal calculus for estimation and control, Nelson Thornes, 1997.
[54] N. Cardoso, J. M. Lemos, Model predictive control of depth of anaesthesia: Guidelines for controller configuration, in: Proc. 30th Annu. Int. Conf. IEEE Engineering in Medicine and Biology Society, Vancouver, BC, Canada, 2008, pp. 5822–5825.
[55] C. M. Ionescu, I. Nasçu, R. D. Keyser, Robustness tests of a model based predictive control strategy for depth of anesthesia regulation in a propofol to bispectral index framework, in: Proc. Int. Conf. Advancements of Medicine and Health Care through Technology, Cluj-Napoca, Romania, 2011, pp. 234–239.
[56] D. D. Ingole, D. N. Sonawane, V. V. Naik, D. L. Ginoya, V. V. Patki, Linear model predictive controller for closed-loop control of intravenous anesthesia with time delay, Int. J. Control Syst. Instrum. 40 (1) (2013) 8–15.
[57] A. Krieger, E. N. Pistikopoulos, Model predictive control of anesthesia under uncertainty, Comput. Chem. Eng. 71 (2014) 699–707.
[58] I. Nasçu, A. Krieger, C. M. Ionescu, E. N. Pistikopoulos, Advanced model-based control studies for the induction and maintenance of intravenous anaesthesia, IEEE Trans. Biomed. Eng. 62 (3) (2015) 832–841.